Hue University Journal of Science: Natural Science
Vol. 130, No. 1B, 21–26, 2021

pISSN 1859-1388
eISSN 2615-9678

MAGNETO-OPTICAL ABSORPTION COEFFICIENTS OF MONOLAYER $MoSe_2$

Tran N. Bich[1,2,3], Huynh V. Phuc[4], Le Dinh[1*]

[1] Center for Theoretical and Computational Physics, University of Education, Hue University, 34 Le Loi St., Hue, Vietnam
[2] Physics Department, University of Education, Hue University, 34 Le Loi St., Hue, Vietnam
[3] Division of Physics, Quang Binh University, Quang Binh, Vietnam
[4] Division of Theoretical Physics, Dong Thap University, Cao Lanh, Dong Thap, Vietnam

* Correspondence to Le Dinh <ledinh@hueuni.edu.vn>
(*Received: 21 January 2021; Accepted: 7 March 2021*)

Abstract. We study the linear, third-order nonlinear, and total absorption coefficients (OACs) caused by intra- and inter-band transitions in monolayer $MoSe_2$ in the presence of a magnetic field by using the compact density matrix approach. The results show that the OACs display the blue-shift behaviour with an increase in the magnetic field. The Zeeman fields do not affect the peak positions but reduce peak intensities slightly. Besides, the strong spin-orbit coupling in monolayer $MoSe_2$ causes the peaks to differ significantly due to spin-up and spin-down. The OACs due to intra-band transition display only one peak in the THz range, while the inter-band spectra show a series of peaks in the near-infrared optical range, making monolayer $MoSe_2$ a promising candidate for novel optoelectronic applications.

Keywords: monolayer $MoSe_2$, magneto-optical absorption coefficients

1 Introduction

Layered materials such as graphene [1], phosphorene [2], silicene [3], germanene [4], and transition-metal dichalcogenides (TMDC) [5, 6] have attracted great interest because of their outstanding properties. These materials are attractive thanks to their fundamental physical properties and great potential applications [7]. With their large natural bandgaps, the TMDCs resolve the gapless problem of graphene, gradually emerging as a potential candidate for new generation materials. That is why the TMCDs have attracted wide attention from scientists in recent years. Among them, monolayer molybdenum diselenide ($MoSe_2$) has been studied increasingly due to its extraordinary properties [8]. $MoSe_2$ has strong spin-orbit-coupling (SOC) with conduction band spin splitting of 0.184 eV and valence band spin splitting of –0.021 eV [9], which provides an excellent system for spin control [10]. In addition, the bandstructure of $MoSe_2$ shows a pair of mismatched valleys at points K and K'. The different conductive and valence bands are spaced by a direct bandgap in the infrared region close to the visible spectrum, which results in an efficient electromagnetic wave absorption and emission.

The linear and nonlinear optical properties of two-dimensional layered materials have been investigated widely in recent years due to their importance for understanding the response of semiconductors stimulated by an electromagnetic field in detail [6, 11, 12]. In this work, we study the linear, third-order nonlinear, and total absorption coefficients (OACs) in monolayer

$MoSe_2$ in a perpendicular magnetic field. We use single-particle eigenfunctions and eigenvalues of this material in the magnetic field. Using the density matrix theory, we calculate the OACs for both intra- and inter-band transitions between the two bands. In Sec. 2, we show the model and the theoretical results. Next, the numerical results and discussion are described in Sec. 3. Finally, we show the conclusion in Sec. 4.

2 Theory

2.1 Single-particle electronic model

We consider a two-dimensional $MoSe_2$ system where carriers move freely in the *(xy)* plane, and a uniform static magnetic field *B* is applied to the *z*-direction. The low-energy Hamiltonian is given as follows:

$$H_0 = v_F(\tau\sigma_x\pi_x + \sigma_y\pi_y) + (\Delta_{\tau,s} + d\Delta_z)\sigma_z + P_{\tau,s} + sM_s - \tau M_v, \quad (1)$$

where $\hbar v_F = 3.11$ (eVÅ) is the Fermi energy [13]; $\sigma_i (i = x, y, z)$ are the Pauli matrices; $\tau = \pm 1$ is the valley index (for K and K′); $s = \pm 1$ is for spin up and spin down; $2d$ is the distance between the Mo and Se sub-lattices; $\Delta_z = eE_z$ with E_z is the electric field applied to the *z*-direction; $\vec{\pi} = \vec{p} + e\vec{A}$ is the canonical momentum with $\vec{p}$ and $\vec{A}$ being the normal momentum and the vector potential. The Dirac mass and the offset energy expressions are [14]

$$\Delta_{\tau,s} = \Delta + s\tau(\lambda_c - \lambda_v)/4, \quad (2)$$

$$P_{\tau,s} = s\tau(\lambda_c + \lambda_v)/4. \quad (3)$$

where $\Delta = 0.74$ eV is the intrinsic band-gap [13]; the Zeeman fields are $M_i = g_i\mu_B B/2$, with $i = s, v$ corresponding to the spin and valley fields; μ_B is the Bohr magneton; $g_i = 2 + g_i^{'}$ with $g_s^{'} = 0.29$ and $g_v^{'} = 3.03$ are the Landé factors [15]. The corresponding eigenvalues of Eq. (1) are

$$E_\lambda = E_{n,s}^{\tau,p} = pE_{n,s}^{\tau} + P_{\tau,s} + sM_s - \tau M_v. \quad (4)$$

Here, $p = \pm 1$ refer to the conduction and valence bands, and

$$E_{n,s}^{\tau} = \sqrt{n(\hbar\omega_c)^2 + (\Delta_{\tau,s}^z)^2}, n = 0, 1, 2, \ldots \quad (5)$$

where $\Delta_{\tau,s}^z = \Delta_{\tau,s} + d\Delta_z$ and $\omega_c = v_F\sqrt{2eB/\hbar}$ is the cyclotron frequency. The eigenfunctions are $|\lambda\rangle = e^{ik_y y}\psi_{n,s}^{\tau,p}(x)/\sqrt{L_y}$,

where

$$\psi_{n,s}^{\tau,p}(x) = \begin{pmatrix} \tau A_{n,s}^{\tau,p}\phi_{n-1}(x - x_0) \\ B_{n,s}^{\tau,p}\phi_n(x - x_0) \end{pmatrix}, \quad (6)$$

with $\phi_n(x)$ being the normalization oscillator functions, and the normalization constants are

$$A_{n,s}^{\tau,p} = \sqrt{\frac{pE_{n,s}^{\tau} + \Delta_{\tau,s}^z}{2pE_{n,s}^{\tau}}}, B_{n,s}^{\tau,p} = \sqrt{\frac{pE_{n,s}^{\tau} - \Delta_{\tau,s}^z}{2pE_{n,s}^{\tau}}}. \quad (7)$$

In the next subsection, we will use the above equations to evaluate the OACs.

2.2 Optical absorption coefficients

Using the compact density matrix approach, we calculate the linear and nonlinear optical susceptibilities for transitions between the two bands $|\lambda\rangle$ and $|\lambda'\rangle$ as follows [6]:

$$\varepsilon_0\chi_{xx}^{(1)}(\Omega) = \frac{1}{2\pi h\alpha_c^2}\sum_{\lambda,\lambda'}\frac{(f_\lambda - f_{\lambda'})(d_{\lambda'\lambda}^x)^* d_{\lambda'\lambda}^x}{E_{\lambda'\lambda} - \hbar\Omega - i\hbar\gamma_0} \quad (8)$$

$$\varepsilon_0\chi_{xx}^{(3)}(\Omega) = -\frac{1}{2\pi h\alpha_c^2}\sum_{\lambda,\lambda'}\frac{(f_\lambda - f_{\lambda'})(d_{\lambda'\lambda}^x)^* d_{\lambda'\lambda}^x}{E_{\lambda'\lambda} - \hbar\Omega - i\hbar\gamma_0} \times\left[\frac{4(d_{\lambda'\lambda}^x)^* d_{\lambda'\lambda}^x}{(E_{\lambda'\lambda} - \hbar\Omega)^2 + (\hbar\gamma_0)^2} - \frac{(d_{\lambda'\lambda'}^x - d_{\lambda\lambda}^x)^2}{(E_{\lambda'\lambda} - i\hbar\gamma)(E_{\lambda'\lambda} - \hbar\Omega - i\hbar\gamma_0)}\right], \quad (9)$$

pISSN 1859-1388
eISSN 2615-9678

where h (3.35 Å) is the thickness of the $MoSe_2$ monolayer [16]; α_c is the magnetic length; $d^x_{\lambda'\lambda} = -e\delta_{k_y,k_y}\left\langle \psi^{\tau',p'}_{n',s'} \middle| x \middle| \psi^{\tau,p}_{n,s} \right\rangle$ is the dipole matrix element in the x-direction, $E_{\lambda'\lambda} = E_{\lambda'} - E_{\lambda}$, $\hbar\gamma_0 = 0.2\sqrt{B}$ (meV) [6]; $\hbar\Omega$ is the photon energy. From the expressions for the optical susceptibilities shown in Eqs. (8) and (9), we can find the OACs as follows [17]:

$$\alpha(\Omega, I) = \alpha^{(1)}(\Omega) + \alpha^{(3)}(\Omega, I), \tag{10}$$

$$\alpha^{(k)}(\Omega, I) = \Omega\sqrt{\frac{\mu}{\varepsilon_R}}\,\mathrm{Im}\left[\varepsilon_0 \chi^{(k)}_{xx}(\Omega)\right]. \tag{11}$$

here, $k = 1, 3$ for the linear and nonlinear terms; μ is the permeability of the material; $\varepsilon_R = n_r^2 \varepsilon_0$ with ε_0 being the permittivity of vacuum; n_r (4.25) is the refractive index; I (3 × 10^6 W/m^2) is the light intensity.

3 Results and discussion

This section provides details for numerical evaluating the linear, nonlinear, and total OACs in monolayer $MoSe_2$. The parameters are shown as they appear.

In Fig. 1, we show the linear OACs caused by the intra-band transition as a function of photon energy, including the effect of the spin and valley Zeeman fields. We can see only one absorption peak for each case of spin. This result is in good agreement with that obtained in monolayer MoS_2 [12], WS_2 [6], and phosphorene [11]. Since the SOC in monolayer $MoSe_2$ is strong, the peak positions due to spin-up and spin-down are separated clearly with slightly higher energy for the spin-up case. Besides, the Zeeman field effect does not change the peak positions but reduces the peak intensities. This behaviour is consistent with that obtained in monolayer WS_2 [6].

In Fig. 2, we show the effect of the electric field on the linear OAC due to intra-band transitions. When the electric field increases, the peak positions shift to the lower-energy region, and the peak intensities decrease. This behaviour might result from the absorbed photon energy caused by the intra-band transition as follows:

$$\hbar\Omega_{\mathrm{intra}} = \frac{(\hbar\omega_c)^2}{2\Delta^z_{\tau,s}} = \frac{(\hbar\omega_c)^2}{2(\Delta_{\tau,s} + d\Delta_z)}. \tag{12}$$

It is clear from Eq. (12) that $\hbar\Omega_{\mathrm{intra}}$ decreases with the increase in the electric field.

Fig. 3 shows the dependence of the linear, third-order nonlinear, and total OACs for intra-band transitions on the photon energy for the spin-up case when B = 10 T, $d\Delta_z$ = 51.25 meV, and M_s and $M_v \neq 0$. Since the third-order nonlinear OAC has a negative value, the total OAC decreases, and this change agrees with what was reported in previous works [6, 11, 12].

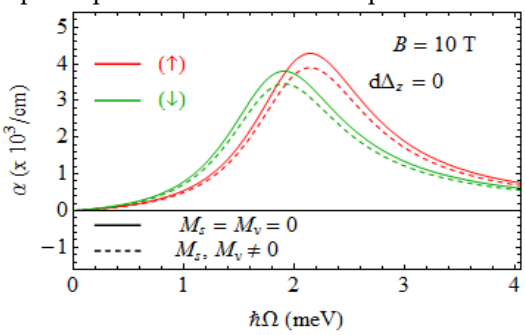

Fig. 1. Linear OAC for intra-band transition versus photon energy when B = 10 T and $d\Delta_z$ = 0 for spin-up and spin-down cases

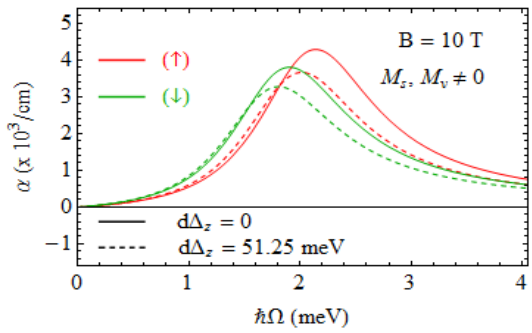

Fig. 2. Linear OAC for intra-band transition versus photon energy when B = 10 T and M_s and $M_v \neq 0$ for two values of the electric field

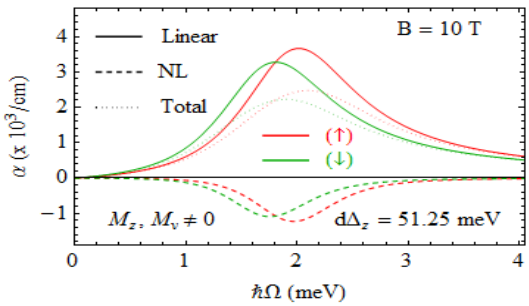

Fig. 3. Linear, third-order nonlinear, and total OACs for intra-band transition versus photon energy when $B = 10$ T, $d\Delta_z = 51.25$ meV, and M_s and $M_v \neq 0$

Since the behaviour of the OACs for spin-up and spin-down cases is the same, in the following, we only evaluate for the spin-up case but the results could be also validated for spin-down one. In Fig. 4, we show the dependence of the linear, third-order nonlinear, and total OACs for intra-band transition versus photon energy for different values of B. It is seen that when the magnetic field increases, the peak positions shift to the higher region of energy. This shift results from the rise in cyclotron energy with the increase in the magnetic field. However, the magnetic field affects the peak intensities of the linear and third-order nonlinear OACs oppositely. While the intensities of the linear OAC increase with the magnetic field, those of the third-order nonlinear OAC decrease. Since the reduction of the peak intensities of the third-order nonlinear OAC is smaller than the increase of the linear OAC, the total OAC increases when the magnetic field increases. This result agrees well with that of monolayer phosphorene [11], WS_2 [6], and conventional low-dimensional structure [18].

We now turn our attention to study the OACs due to inter-band transition. Fig. 5 shows the linear, third-order nonlinear, and total OACs dependence on the photon energy. The calculations are presented for the spin-up case at a particular value of $d\Delta_z$ and when M_s and $M_v \neq 0$. Unlike in the intra-band transition cases where only one peak at the THz region appear in the absorption spectra, a series of peaks appear in the absorption spectra at the near-infrared region due to inter-band transition. This appearance might result from the expression of the absorbed photon energy as follows:

$$\hbar\Omega_{inter} = \frac{(2n+1)(\hbar\omega_c)^2}{2(\Delta_{\tau,s} + d\Delta_z)} + 2(\Delta_{\tau,s} + d\Delta_z). \qquad (13)$$

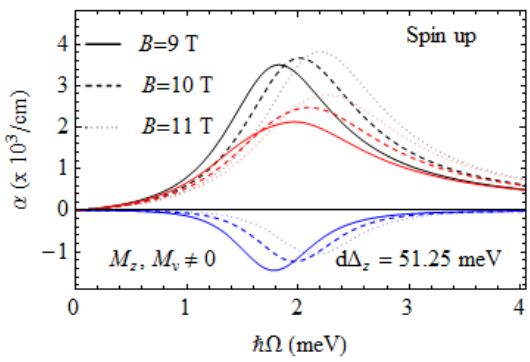

Fig. 4. Linear, third-order nonlinear, and total OACs for intra-band transition versus photon energy for different values of B. The results are calculated for the spin-up case when $d\Delta_z = 51.25$ meV, and M_s and $M_v \neq 0$.

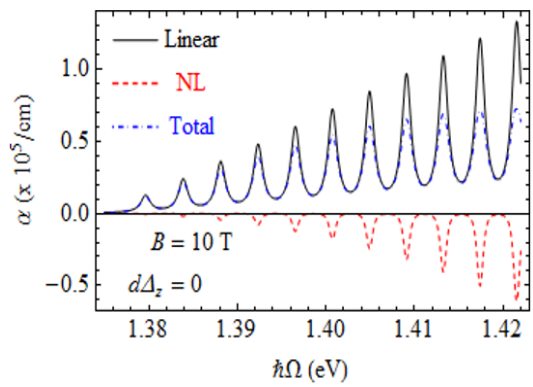

Fig. 5. Linear, third-order nonlinear, and total OACs for inter-band transition versus photon energy. The results are calculated for the spin-up case when $B = 10$ T, $d\Delta_z = 0$, and M_s and $M_v \neq 0$.

pISSN 1859-1388
eISSN 2615-9678

It is clear that $\hbar\Omega_{inter}$ is proportional to $(2n + 1)$, leading to the overlapped behaviour of the resonant peaks but gradually shifts to the higher-energy region with the increase of the Landau levels. That is the reason why the absorbed spectra appear in a series of peaks. For the peak positions, we see that $\hbar\Omega_{inter} \propto 2\Delta_{\tau,s}$, whose value is at the near-infrared region. Besides, the peak intensities due to the inter-band transitions are much higher than those due to intra-band transitions. These results also agree well with those obtained in the monolayer WS_2 [6] and MoS_2 [12].

Like Fig. 5, Fig. 6 shows the OACs when $d\Delta z$ = 51.25 meV. When the electric field is taken into account, the absorption spectra system shifts to the higher-energy region. This can be seen clearly from Eq. (13), which shows the absorbed photon energy is proportional to the electric field.

The influence of the magnetic field on the OACs due to inter-band transition is shown in Fig. 7. We can see that the peak positions shift to the higher-energy region because the cyclotron energy increases with the magnetic field. This result is consistent with that reported in the monolayer WS_2 [6] and MoS_2 [12].

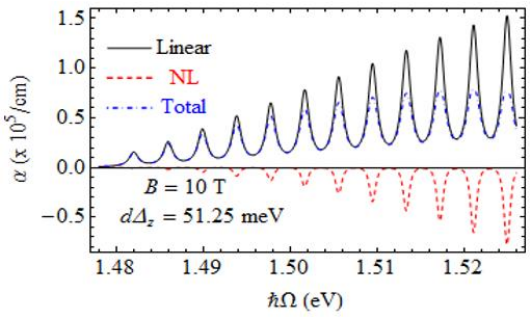

Fig. 6. The linear, third-order nonlinear, and total OACs for inter-band transition versus photon. The results are calculated for the spin-up case when B = 10 T, $d\Delta_z$ = 51.25 meV, and M_s and $M_v \neq 0$.

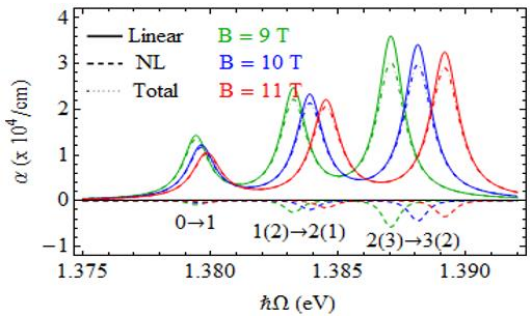

Fig. 7. Linear, third-order nonlinear, and total OACs for inter-band transition versus photon for different values of B. The results are calculated for the spin-up case when $d\Delta_z = 0$ and M_s and $M_v \neq 0$.

4 Conclusion

We have studied the linear, third-order nonlinear, and total OACs in the monolayer $MoSe_2$ in the presence of a perpendicular magnetic field. The results are also calculated when the electric and the Zeeman fields are taken into account. Our results show that the absorption spectrum appears in two different regions depending on the intra-band or inter-band transitions. While the OACs due to the intra-band transition have only one peak at the THz region, the OACs due to the inter-band transition possess a series of peaks at the near-infrared region. Furthermore, the effect of the Zeeman field and the electric field on the OACs is different: while the Zeeman field does not change the peak positions, the electric field shifts the peak positions due to the intra/inter-band transition to the lower/higher-energy region. Besides, strong SOC in the monolayer $MoSe_2$ causes the absorption peaks due to the spin-up and the spin-down to separate. Our theoretical results provide the potential of $MoSe_2$ as a promising material for designing nano-electronic and optical devices.

Funding statement

Tran N. Bich is funded by Vingroup Joint Stock Company and supported by the Domestic Master/PhD Scholarship Programme of Vingroup Innovation Foundation (VINIF), Vingroup Big Data Institute (VINBIGDATA), code VINIF.2020. TS.72.

This research is funded by the Vietnam National Foundation for Science and Technology Development (NAFOSTED) under Grant No. 103.01-2019.11.

References

1. Novoselov KS, Jiang D, Schedin F, Booth T, Khotkevich V, Morozov S, Geim AK. Two-dimensional atomic crystals. Proceedings of the National Academy of Sciences. 2005;102(30):10451-3.
2. Tahir M, Vasilopoulos P, Peeters FM. Magneto-optical transport properties of monolayer phosphorene. Physical Review B. 2015;92(4):045420.
3. Chen L, Liu C-C, Feng B, He X, Cheng P, Ding Z, et al. Evidence for Dirac fermions in a honeycomb lattice based on silicon. Physical Review Letters. 2012;109(5):056804.
4. Chen X, Yang Q, Meng R, Jiang J, Liang Q, Tan C, et al. The electronic and optical properties of novel germanene and antimonene heterostructures. Journal of Materials Chemistry C. 2016;4(23):5434-41.
5. Hien ND, Nguyen CV, Hieu NN, Kubakaddi S, Duque C, Mora-Ramos M, et al. Magneto-optical transport properties of monolayer transition metal dichalcogenides. Physical Review B. 2020;101(4): 045424.
6. Huong PT, Muoi D, Bich TN, Phuc HV, Duque C, Nguyen PTN, et al. Intra-and inter-band magneto-optical absorption in monolayer WS_2. Physica E: Low-dimensional Systems and Nanostructures. 2020;124:114315.
7. Mak KF, Shan J. Photonics and optoelectronics of 2D semiconductor transition metal dichalcogenides. Nature Photonics. 2016;10(4):216-26.
8. Yong C-K, Horng J, Shen Y, Cai H, Wang A, Yang C-S, et al. Biexcitonic optical stark effects in monolayer molybdenum diselenide. Nature Physics. 2018;14(11):1092-6.
9. Liu G-B, Shan W-Y, Yao Y, Yao W, Xiao D. Three-band tight-binding model for monolayers of group-VIB transition metal dichalcogenides. Physical Review B. 2013;88(8):085433.
10. Novoselov KS, Geim AK, Morozov SV, Jiang D, Zhang Y, Dubonos SV, et al. Electric field effect in atomically thin carbon films. Science. 2004;306(5696):666-9.
11. Nguyen CV, Hieu NN, Duque CA, Khoa DQ, Hieu NV, Tung LV, et al. Linear and nonlinear magneto-optical properties of monolayer phosphorene. Journal of Applied Physics. 2017;121(4):045107.
12. Nguyen CV, Hieu NN, Muoi D, Duque CA, Feddi E, Nguyen HV, et al. Linear and nonlinear magneto-optical properties of monolayer MoS_2. Journal of Applied Physics. 2018;123(3):034301.
13. Xiao D, Liu G-B, Feng W, Xu X, Yao W. Coupled spin and valley physics in monolayers of MoS_2 and other group-VI dichalcogenides. Physical Review Letters. 2012;108(19):196802.
14. Catarina G, Have J, Fernández-Rossier J, Peres NM. Optical orientation with linearly polarized light in transition metal dichalcogenides. Physical Review B. 2019;99(12):125405.
15. Kormányos A, Zólyomi V, Drummond ND, Burkard G. Spin-orbit coupling, quantum dots, and qubits in monolayer transition metal dichalcogenides. Physical Review X. 2014;4(1): 011034.
16. Ding Y, Wang Y, Ni J, Shi L, Shi S, Tang W. First principles study of structural, vibrational and electronic properties of graphene-like MX_2 (M= Mo, Nb, W, Ta; X= S, Se, Te) monolayers. Physica B: Condensed Matter. 2011;406(11):2254-60.
17. Rezaei G, Karimi M, Keshavarz A. Excitonic effects on the nonlinear intersubband optical properties of a semi-parabolic one-dimensional quantum dot. Physica E: Low-dimensional Systems and Nanostructures. 2010;43(1):475-81.
18. Gambhir M, Kumar M, Jha P, Mohan M. Linear and nonlinear optical absorption coefficients and refractive index changes associated with intersubband transitions in a quantum disk with flat cylindrical geometry. Journal of luminescence. 2013;143:361-7.